Quantifying snowfall from orographic cloud seeding

Katja Friedrich[a,1], Kyoko Ikeda[b], Sarah A. Tessendorf[b], Jeffrey R. French[c], Robert M. Rauber[d], Bart Geerts[c], Lulin Xue[b], Roy M. Rasmussen[b], Derek R. Blestrud[e], Melvin L. Kunkel[e], Nicholas Dawson[e], and Shaun Parkinson[e]

[a]Department of Atmospheric and Oceanic Sciences, University of Colorado Boulder, Boulder, CO 80309; [b]Research Applications Laboratory, National Center for Atmospheric Research, Boulder, CO 80307; [c]Department of Atmospheric Science, University of Wyoming, Laramie, WY 82071; [d]Department of Atmospheric Sciences, University of Illinois at Urbana–Champaign, Urbana, IL 61820; and [e]Cloud Seeding Group, Idaho Power Company, Boise, ID 83702

Edited by John H. Seinfeld, California Institute of Technology, Pasadena, CA, and approved January 30, 2020 (received for review October 2, 2019)

Climate change and population growth have increased demand for water in arid regions. For over half a century, cloud seeding has been evaluated as a technology to increase water supply; statistical approaches have compared seeded to nonseeded events through precipitation gauge analyses. Here, a physically based approach to quantify snowfall from cloud seeding in mountain cloud systems is presented. Areas of precipitation unambiguously attributed to cloud seeding are isolated from natural precipitation (<1 mm h^{-1}). Spatial and temporal evolution of precipitation generated by cloud seeding is then quantified using radar observations and snow gauge measurements. This study uses the approach of combining radar technology and precipitation gauge measurements to quantify the spatial and temporal evolution of snowfall generated from glaciogenic cloud seeding of winter mountain cloud systems and its spatial and temporal evolution. The results represent a critical step toward quantifying cloud seeding impact. For the cases presented, precipitation gauges measured increases between 0.05 and 0.3 mm as precipitation generated by cloud seeding passed over the instruments. The total amount of water generated by cloud seeding ranged from 1.2 × 10^5 m^3 (100 ac ft) for 20 min of cloud seeding, 2.4 × 10^5 m^3 (196 ac ft) for 86 min of seeding to 3.4 x 10^5 m^3 (275 ac ft) for 24 min of cloud seeding.

clouds | precipitation | cloud seeding | radar observations | gauge observations

Wintertime mountain cloud systems have been seeded to increase snowpack and water supplies since the discovery (1) that ice crystals could be generated by injecting silver iodide (AgI) into a cloud of supercooled liquid (2). During this process, termed glaciogenic seeding, AgI aerosols are introduced into a supercooled liquid cloud to nucleate ice crystals, which then achieve sizes and fall velocities sufficient to fall to the surface.

To date, studies quantifying the impact of glaciogenic seeding of orographic clouds have employed statistical comparisons between seeded and nonseeded events and times as well as target and control areas (2). Physical process studies attempt to track or identify seeding plumes and associate enhancements in snowfall to quantifying seeding impacts. Reported enhancements in snowfall due to cloud seeding range between 0.5 and 2 mm h^{-1} (3–6), and enhancements in reflectivity echoes unambiguously attributed to cloud seeding have been reported in a handful of studies (3, 7). All of these studies are often challenged by the difficulty in distinguishing between natural and seeded precipitation, nonrepeatability of a controlled experiment in nature, and the detection of a relatively small signal in weather systems exhibiting large natural variability (2). While most studies using a statistical approach remain inconclusive about the amount of precipitation generated by cloud seeding (2), a few overcome the challenges and show statistically significant increases in snowfall (8) or use a computer-intensive ensemble technique to evaluate cloud seeding through the use of thousands of model simulations (9). What makes this study unique is that 1) the temporal evolution of a seeded cloud is documented from the time of AgI injection to the time of snowfall on the ground, over the full width of the seeded cloud parcel, and 2) the seeding-induced snowfall is isolated unambiguously from natural precipitation. Instead of traditional statistical comparisons, we introduce here a physically based approach by which we isolate areas of precipitation that were unambiguously generated by cloud seeding and quantify the amount of precipitation in these areas using precipitation gauge measurements and ground-based radar analyses. This approach is applied to radar echoes that were attributed to seeding at a time of no or light (<1 mm h^{-1}) natural precipitation for three cloud seeding events. This study combines radar and gauge analyses in order to quantify the spatial and temporal evolution of snowfall from cloud seeding.

For the three cases presented, unambiguous evidence was provided in two studies (10, 11) that glaciogenic seeding from an aircraft led to the production of precipitation that eventually fell to the surface. However, the amount of precipitation produced for the three cases was not quantified in these previous studies, which would be a fundamental step toward investigating cloud seeding efficacy. Cloud seeding efficacy depends on the type of cloud seeding operations and the temporal and spatial evolution of a variety of atmospheric variables that control microphysical and dynamical processes in clouds and precipitation. Here, we quantify snowfall accumulation from glaciogenic cloud seeding and its spatial and temporal evolution based on radar observations and snow gauge measurements. The data were obtained during 3 d in 2017 (19 January, 20 January, and 31 January), when orographic clouds were seeded with AgI released from aircraft in the Payette basin of Idaho during the Seeded and

Significance

Cloud seeding to increase winter snowpack in mountains has traditionally been evaluated using precipitation gauges and target/control statistics leading mostly to inconclusive results. Here, an approach employing radar and gauges is used to quantify snowfall by first isolating radar returns that are unambiguously the result of cloud seeding in regions with light or no natural precipitation and then quantifying the seeding-induced precipitation at the ground. The spatiotemporal evolution of snowfall from cloud seeding is quantified. Although this study focuses only on three cases, the results are a fundamental step toward understanding cloud seeding efficacy that, for over half a century, has been an unanswered question for water managers wishing to utilize the technology for water resource management.

Author contributions: K.F., S.A.T., J.R.F., R.M. Rauber, B.G., L.X., R. M. Rasmussen, D.R.B., M.L.K., N.D., and S.P. designed research; K.F., K.I., S.A.T., J.R.F., R.M. Rauber, B.G., L.X., R. M. Rasmussen, D.R.B., M.L.K., N.D., and S.P. performed research; K.F., K.I., and S.A.T. contributed new reagents/analytic tools; K.F. and K.I. analyzed data; and K.F., S.A.T., J.R.F., R.M. Rauber, B.G., L.X., R. M. Rasmussen, D.R.B., M.L.K., and S.P. wrote the paper.

The authors declare no competing interest.

This article is a PNAS Direct Submission.

[1]To whom correspondence may be addressed. Email: katja.friedrich@colorado.edu.

This article contains supporting information online at https://www.pnas.org/lookup/suppl/doi:10.1073/pnas.1917204117/-/DCSupplemental.

First published February 24, 2020.

Natural Orographic Wintertime Clouds: The Idaho Experiment (SNOWIE) (11). On all 3 d, both burn-in-place and ejectable flares were used to release AgI from a seeding aircraft. The aircraft flew repeated ∼50-km-long tracks, perpendicular to the mean wind and upwind of the observational domain. Exact track locations and altitudes dependended on wind direction, speed, and cloud conditions. Tracks, with approximately the same amount of AgI, were repeated six times on 19 January, eight times on 20 January, and two times on 31 January (11).

Results and Discussion

Snow Accumulation at Gauge Sites. On 19 January, airborne cloud seeding began at 1619 UTC. Two seeding lines passed over the precipitation gauges at Five Corners and Silver Creek, located within the area covered by the radars, termed the radar observational domain (ROD; Fig. 1) and eventually over the Banner gauge site, located 67 km east of the Packer John radar site outside of the ROD. Although, a network of precipitation gauges was deployed, gauge data were included in this study only if they met the quality standards described in the *SI Appendix* and seeding lines passed over the gauge. Between 1640 and 1710 UTC light snowfall with a mean rate of about 1.3 mm h^{-1} (0.6 mm h^{-1}) was observed at Five Corners (Silver Creek and Banner; Fig. 2*A*). Patches of natural, light precipitation surrounded the seeding lines as they passed through the ROD. These patches were readily detected by the radars with equivalent radar reflectivity factor (Z_e) values ranging between 1 and 15 dBZ_e (Fig. 1*A* and *SI Appendix*, Movie S1). Based on radar analyses, the two seeding lines passed over the Five Corners site between 1710 and 1722 UTC (Fig. 2*B* and *SI Appendix*, Movie S1). Between 1719 and 1724 UTC, a steep increase in accumulation rate was observed by the Five Corners gauge (Fig. 2*A*, red line). Since the increase in precipitation accumulation from the gauge coincides with the time that the seeding lines passed over the gauges, we conclude that the precipitation accumulation observed by the gauge was related to the precipitation generated through cloud seeding. A total of 0.2 mm accumulated during the 5 min when the seeding lines passed over the instrument. Removing the mean accumulation rate of 1 mm h^{-1} measured 5 min prior and after the passage of the seeding lines, we attribute about 0.1 mm (1.2 mm h^{-1}) to the effect of cloud seeding. SD in snowfall rate before and during seeding is about 0.3 and 0.4 mm h^{-1}, respectively, indicating that the increase due to seeding is three to four times greater than the apparent natural variability.

As the lines propagated downwind, the first seeding line passed over the Silver Creek gauge between 1734 and 1740 UTC based on the radar analysis (Fig. 2*B* and *SI Appendix*, Movie S1). For 20 min prior, until 1736 UTC, no precipitation was observed by the Silver Creek gauge. The second seeding line passed over the instrument between 1741 and 1746 UTC as seen in Fig. 2*B*. Between 1736 and 1746 UTC, the gauge showed a slight increase in precipitation accumulation (Fig. 2*A*) amounting to a total of

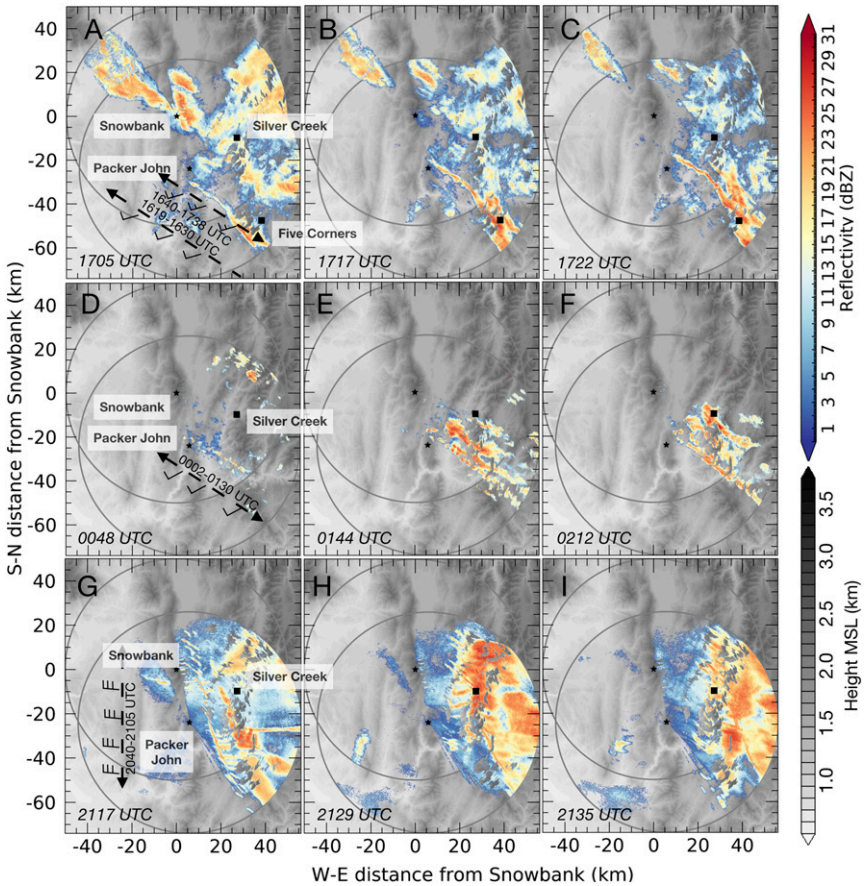

Fig. 1. Maximum Z_e between the surface and 1 km AGL within the ROD for selected times on (*A*–*C*) 19 January based on the merged Z_e from both radars; (*D*–*F*) 20 January from the Packer John radar; and (*G*–*I*) 31 January 2017 from the Packer John (PJ) radar. Gauge data were included in this study only if they met the quality standards and seeding lines passed over the gauge (*SI Appendix*). Location of the precipitation gauges at Silver Creek on 19, 20, and 31 January and Five Corners on 19 January and radars at Packer John and Snowbank (SB) are indicated as square and star symbols, respectively. Gray circles centered on the radars indicate the maximum range. Seeding aircraft flight track, time of seeding, and wind at flight level appear on *A*, *D*, and *G* (half barb: 2.5 m s^{-1} and full barb: 5 m s^{-1}).

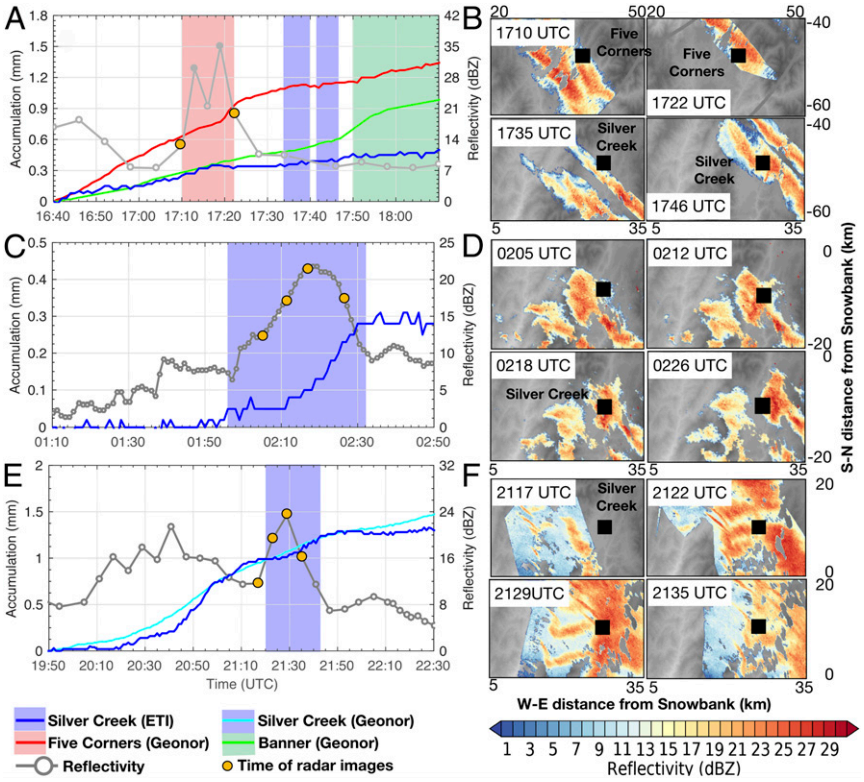

Fig. 2. Radar and precipitation observations at the gauge sites for (*A* and *B*) 19 January showing 1-min accumulated precipitation at Silver Creek, Five Corners, Banner and 6-min Z_e observed by PJ radar at 1° at the Five Corners site (*Left*) and Z_e at 1° elevation angle in the vicinity of Five Corners and Silver Creek during seeding line passage (*Right*); (*C* and *D*) 20 January showing 1-min accumulated *S* and 1-min Z_e observed by PJ radar at 1° at Silver Creek (*Left*) and Z_e at 1° around the Silver Creek site during seeding line passage (*Right*); and (*E* and *F*) 31 January showing 1-min *S* from the Geonor and ETI gauge and 6-min Z_e at 1° at Silver Creek (*Left*) and Z_e at 1° around Silver Creek during the seeding line passage (*Right*). (*Left*) Periods when seeding lines passed over the gauge sites based on radar analysis are color coded. Times of Z_e observations (extrapolations) are indicated as open (closed) circles in *Left*. Times of radar observations at Five Corners in *B* and Silver Creek in *D* and *F* shown in the *Right* are indicated as yellow circles in the *Left*. Panels *B*, *D*, and *F* only show Z_e associated with the seeding lines; method to isolate the seeding lines is described in the *SI Appendix* and shown in *SI Appendix*, Movies S1–S3.

about 0.05 mm. It is not possible to attribute this increase to the passage of either the first or second seeding line (or both) as these increases are small and lie within the uncertainty bounds of the precipitation observations (±0.1 mm). Airborne radar observations (10) indicate that the first seeding line may not have reached the surface at Silver Creek, while the second seeding line, producing light surface snowfall with $Z_e < 5$ dBZ$_e$, had already reached the surface at 1730 UTC, upwind of Silver Creek.

By 1750 UTC, the seeding lines moved out of the ROD and approached the Banner gauge site. Here, we use the propagation speed of the seeding lines within the ROD to estimate the time the lines passed over Banner. Assuming a radar-estimated propagation speed of 43 km h^{-1}, the lines were expected to pass over the Banner gauge between 1750 and 1810 UTC (Fig. 2*A*, green shaded area). The gauge shows a distinct increase in precipitation accumulation of 0.2 mm (0.86 mm h^{-1} with an SD of 0.4 mm h^{-1}) between 1746 and 1800 UTC compared to the mean precipitation accumulation rate of 0.43 mm h^{-1} (SD of 0.2 mm h^{-1}) prior to and after the seeding lines' passage (Fig. 2*A*, green line). The passage of the seeding lines took 14 min, during which time 0.1 mm of natural precipitation occurred. Therefore, subtracting that from the 0.2-mm accumulation during seeding line passage yields 0.1 mm of precipitation attributed to cloud seeding. Although the precipitation accumulations at Banner and Five Corners are quite similar (0.1 mm), the duration of the increase in precipitation lasted longer (~14 min) at Banner compared to ~5 min at Five Corners, a consequence of the horizontal dispersion of the precipitation particles with distance downwind from the seeding location. As a result, the precipitation rate was less at Banner compared to Five Corners. While light snowfall would have been observed without cloud seeding on 19 January, the gauge analysis indicates that snowfall from the seeded clouds almost doubled the snowfall rate at Banner and Five Corners.

On 20 January, radar observations indicate almost no snowfall ($Z_e < 0$ dBZ$_e$) from natural clouds. Patches of enhanced reflectivity ($Z_e < 10$ dBZ$_e$) surrounding the northern end of the lines were observed between 0000 and 0200 UTC (*SI Appendix*, Movie S2). Two of the eight seeding lines observed by the radar passed over the Silver Creek site, the only gauge site with a seeding line passage and that met the quality standards on 20 January (*SI Appendix*). The lines merged on the northwesternmost end of the lines before passing over the gauge site. The remaining six seeding lines precipitated out before reaching Silver Creek (Fig. 1 *D*–*F* and *SI Appendix*, Movie S2). The set of merged lines passed over the gauge site between 0154 and 0232 UTC (Fig. 2 *C* and *D*). The Silver Creek gauge measured an increase in precipitation between 0156 and 0230 UTC, before and after which no precipitation was detected (Fig. 2*C*, blue line). A total of 0.28 mm accumulated during the 38 min the seeding lines passed over the instrument, resulting in a mean precipitation rate of 0.44 mm h^{-1}. Gauge and radar analyses indicate that snowfall between 0000 and 0300 UTC in the ROD can be attributed to cloud seeding. Natural clouds would not have produced any snowfall in the ROD during this time.

On 31 January, enhanced Z_e from two seeding lines (>20 dBZ$_e$) were detected. The lines are surrounded by natural clouds with Z_e mainly ranging between 1 and 10 dBZ$_e$. Isolated areas of enhanced

Z_e up to 20 dBZ_e associated with natural clouds were observed in the northeastern part of the ROD. The northern end of the two seeding lines passed over the Silver Creek site between 2120 and 2142 UTC (Figs. 1 *G–I* and 2 *E* and *F* and *SI Appendix*, Movie S3). Only observations at Silver Creek met the quality standards described in *SI Appendix*. The lines were propagating quickly and at that time had already merged. As such, the radar analysis was unable to distinguish the passage of individual lines. During this event each seeding leg utilized both burn-in-place and ejectable flares (11). Strong vertical wind shear greater than 10^{-2} s^{-1} initially led to a horizontal separation of about 10 km (Fig. 1*G*) between areas of enhanced Z_e resulting from burn-in-place flares (wide lines of continuous enhanced Z_e; Fig. 1*G* and *SI Appendix*, Movie S3) and those resulting from ejectable flares (comma shapes trailing the main line of enhanced Z_e; Fig. 1*G* and Movie S3). On this day, two types of gauges were deployed at Silver Creek (*SI Appendix*) both measuring light snowfall prior to the passage of the seeding lines with slight differences in their measured precipitation rate. The first gauge indicated snowfall of <1 mm h^{-1} between 2020 and 2115 UTC (Fig. 2*E*), before the snowfall stopped at 2115 UTC. Corresponding to the time of seeding line passage, the gauge measured increased snowfall between 2125 and 2150 UTC before snowfall stopped again at 2150 UTC. The gauge did not appear to resolve precipitation-related burn-in-place and ejectable flares separately. Inspection of the radar data suggests that radar echoes resulting from the ejectable flares, visible as comma-shaped maxima in Z_e, were not reaching the ground as they passed over the gauge site. Since no snowfall occurred before 2125 UTC, nor after 2150 UTC, the increase of 0.25 mm (0.6 mm h^{-1}) in snow accumulation is attributed solely to the passage of the seeding lines. The SD of snowfall rate during seeding is 0.4 mm h^{-1}. The collocated second gauge measured precipitation accumulation that compared very well with the first (Fig. 2*E*). However, the second gauge observed almost continuous snowfall (0.6 mm h^{-1}) between 2100 and 2150 UTC with a slight decrease in accumulation rate after 2150 UTC, wich was the end of the seeding line passage. There was no noticeable increase in snow accumulation rate during the seeding line passage between 2125 and 2150 UTC, as observed by the first gauge. This suggests that the snow accumulation signal from these seeding lines is quite small and often within the uncertainty of the gauge measurement. Nonetheless, given the clear passage of these lines in the radar data, we are confident with the times of their passage and that precipitation in particular from the first gauge from this time was due to seeding. Gauge and radar analyses suggest that natural clouds produced light snowfall of <1 mm h^{-1} on 31 January. There was increase in snowfall rate in the first gauge as the seeding lines passed through the ROD.

Spatial Distribution and Total Amount of Snow Accumulation. To quantify the amount of precipitation generated through cloud seeding and determine its distribution across the ROD, measurements from two ground-based radars (Fig. 1) are combined to estimate snowfall rates based on relationships between Z_e and liquid equivalent snowfall rate, S. Only Z_e associated with seeding lines between the surface and 1 km above ground level are used. Signals not attributed to seeding (i.e., natural precipitation) were removed manually. This technique minimizes the impact of snowfall from natural clouds outside the seeding lines. We acknowledge that the seeded clouds could have produced snowfall had they not be seeded. However, gauge and radar analyses showed that the signal from the natural clouds nearby is less than that from the seeded clouds. Animations of each of the three cases of the observed and processed Z_e are provided in *SI Appendix*, Movies S1–S3; details on radar operations and data processing appear in the *SI Appendix*.

Distribution maps of accumulated snowfall were generated by applying a Z_e–S relationship ($Z_e = aS^b$) to each radar scan timestep and integrating S with each timestep as the seeding lines pass through the ROD. A thorough analysis was conducted to establish a relationship for each day that best represents snowfall from the seeding lines based on precipitation gauge observations, hereafter referred to as the best-match relationship (*SI Appendix*, Fig. S1). Since Z_e–S relationships depend on snow characteristics, a single relationship is unlikely to accurately represent the snowfall rate (12). To address the Z_e–S related uncertainty, an ensemble of Z_e–S relationships was also developed by varying the coefficient a between 100 and 500 (in steps of 1) and the exponent b between 2 and 2.2 (in steps of 0.1). The range of these coefficients is based on Z_e–S relationships from the literature (13–17). From the ensemble it is possible to calculate percentile values, providing an uncertainty estimate for the radar-derived precipitation. We calculated ensemble percentiles based on Z_e measured at the gauge sites to complement the best-match Z_e–S relationship (Fig. 3 and Table 1) and Z_e measured over the entire ROD (Fig. 4).

Domainwide accumulated snowfall resulting only from the seeding lines are shown in Fig. 3. On 19 January, seeding-induced snowfall was almost equally distributed from each line as the seeding lines passed through the ROD with slightly greater accumulations over the higher terrain. Note that the seeding lines were detected prior to 1705 UTC by the airborne radar, but were not visible by the ground-based radar due to radar beam blockage south of Packer John. Gaps between lines are related to the 6-to-7-min sampling interval of the radars on this day. Holes in accumulated snowfall, such as those apparent just west of Five Corners (Fig. 3*A*), are due to the removal of data contaminated by ground clutter. Most of the seeding-induced snowfall on 20 January appeared confined to the southeastern portion of the ROD (Fig. 3*B*). On this day, lighter winds and faster fallout of the precipitation provided a much better resolved surface precipitation field compared to 19 January. For the day with the strongest winds (31 January; Fig. 3*C*), much of the snowfall occurred in the eastern most portion of the ROD and one might conjecture that additional snow fell to the east, outside the ROD.

On 19 January, snow resulting from the seeding lines began to reach the surface at 1705 UTC and continued through 1812 UTC (Fig. 3*A*). Using the best-match Z_e–S relationship for that day, less than 0.15 mm accumulated at each radar pixel (100 × 100 m) through the entire period. The highest accumulations occurred over higher terrain suggesting that snowfall was enhanced through orographic lift. As the seeding lines interacted with the higher terrain, the area of enhanced Z_e also widened (*SI Appendix*, Movie S1), covering an area of about 40 to 90 km^2 between 1705 and 1716 UTC (Fig. 1 *A–C* and *SI Appendix*, Movie S1) to 130 km^2 at 1804 UTC. Using the best-match Z_e–S relationship, a total of 123,220 m^3 (~100 ac ft) of liquid equivalent snowfall

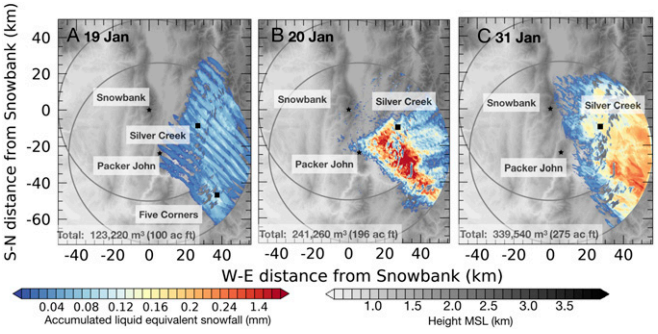

Fig. 3. Distribution of accumulated liquid equivalent snowfall (*S*) attributed to cloud seeding over the observational period between (*A*) 1705 and 1806 UTC on 19 January; (*B*) 0042 and 0315 UTC on 20 January; and (*C*) 2117 and 2151 UTC on 31 January 2017 using the best-match Z_e–S relationship for that day. Data are shown on a 100 × 100 m grid. Total accumulations over the entire domain and observational period are highlighted. Corresponding Z_e are shown in *SI Appendix*, Movies S1–S3.

Table 1. List of Z_e–S ensemble members ($Z_e = a\,S^b$) based on Z_e observed after the seeding lines passed Five Corners on 19 January and Silver Creek on 20 and 31 January

	19 January	20 January	31 January
Best match	228 $S^{2.1}$	234 S^2	165 $S^{2.2}$
5th percentile	495 S^2	491 $S^{2.1}$	445 S^2
25th percentile	387 $S^{2.1}$	352 $S^{2.0}$	420 $S^{2.2}$
75th percentile	162 $S^{2.1}$	171 $S^{2.2}$	169 $S^{2.2}$
95th percentile	81 S^2	71 $S^{2.0}$	72 $S^{2.1}$

Best match is the minimum between radar-based S and gauge observation with <0.05-mm differences

accumulated over the 67 min over an area of 2,327 km^2 resulting from two seeding lines or 20 min of seeding (Fig. 3*A*). Uncertainties related to the choice of Z_e–S relationship, estimated from the 25th and 75th (5th and 95th) percentile (Table 1), range from 95,776 to 144,994 m^3 (78,582 to 194,261 m^3). Comparing the Z_e–S relationship ensemble to the best match leads to differences in snow accumulation of about ±20% (±47%) using the 25th/75th (5th/95th) percentiles Z_e–S relationship compared to the best-match Z_e–S relationship (Table 1).

Next, we investigate how snowfall rate varies by examining the percentile of snowfall estimates based on all of the Z_e–S relationships within the ensemble for each radar scan time. As the seeding lines passed through the ROD on 19 January, the total areal snowfall accumulation within the ROD ranged between about 4,000 and 19,000 m^3 (3.2 and 15.4 ac ft) following the seven Z_e–S relationships (Fig. 4*A*, colored lines). The 5th and 95th percentile for every radar scan from the Z_e–S ensemble ranged between 4,000 and 24,000 m^3 (3.2 and 19.4 ac ft). Total accumulations increased between 1705 and 1746 UTC with larger accumulations between 1722 and 1746 UTC. For instance, the total accumulation based on the best-match relationship doubled from 7,000 m^3 (5.7 ac ft) at 1722 UTC to 14,000 m^3 (11.4 ac ft) at 1746 UTC. After 1753 UTC, accumulations slowly decreased as the lines left the ROD. This suggests that the seeding-induced snowfall increases with time and as the seeding lines passed over the higher terrain. As the snowfall rate within the lines increased, the areal coverage also increased (Fig. 4, star symbols). For this day, the area covered by the seeding lines increased from 200 to 410 km^2 between 1705 and 1758 UTC (Fig. 4*A*, star symbols) and decreased to 224 km^2 as the seeding lines moved out of the ROD at 1806 UTC.

On 20 January, snow accumulated mostly within the ROD about 5 to 30 km east of Packer John within a ~20-km swath perpendicular to the southwesterly flow (Fig. 3*B*). Total accumulation was mostly less than 1.5 mm at each individual radar pixel. Initially, seeding lines were narrow. They started to broaden quickly and merge with other seeding lines due to the low wind speed. Most of the seeding lines precipitated out before reaching the highest terrain. A total of 241,260 m^3 (~196 ac ft) of liquid equivalent snowfall accumulated during the 160 min over an area of 1,838 km^2 resulting from eight seeding lines or 86 min of cloud seeding. The total snowfall based on the ensemble varied by 20% to 80% compared to the best-match relationship. This relates to total S ranging between 196,319 and 312.521 m^3 (179,986 and 437,125 m^3) considering the 25th and 75th (5th/95th) percentile of the ensemble. Compared to 19 January, almost double the amount of snow was distributed over a much smaller area and throughout a much longer time period on 20 January.

Contrary to 19 January, most of the snow fell within the ROD with up to 280,00 m^3 of accumulations (22.7 ac ft; Fig. 4*B*) following the published Z_e–S relationships (Fig. 4*B*, colored lines). Considering the Z_e–S ensemble, the 5th/95th percentile estimates reached up to 34,000 m^3 (27.6 ac ft). Accumulations increased between 0042 and 0123 UTC, remained almost steady until 0212 UTC and decreased until all snow reached the ground at 0315 UTC. The areal coverage of precipitation at a given time from the seeding lines steadily increased from 140 to 550 km^2 between 0034 and 0123 UTC, remained above this value until 0158 UTC, and

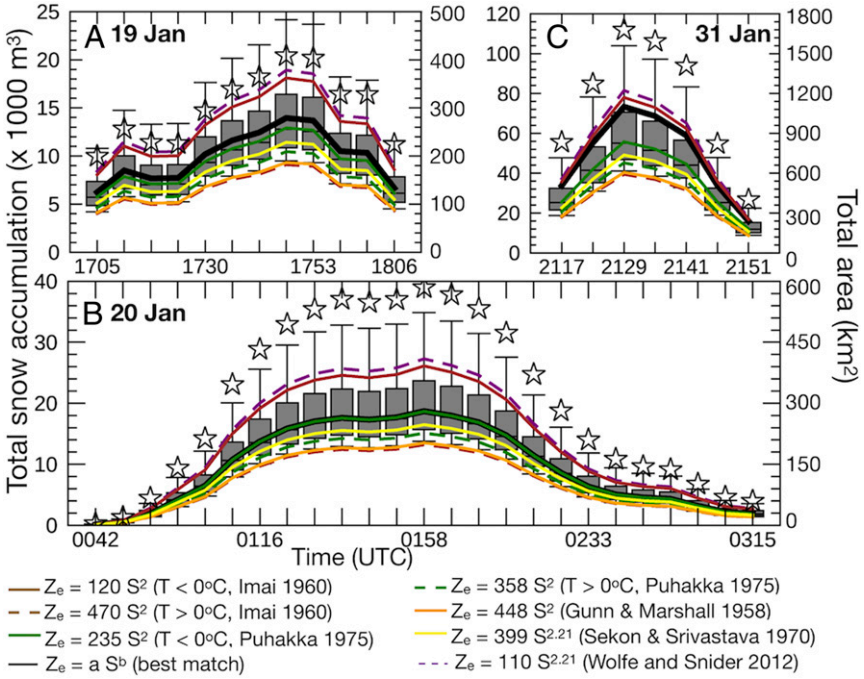

Fig. 4. Total accumulated S over the ROD for each radar volume on (*A*) 19 January using the SB and PJ radars; (*B*) 20 January using the PJ radar; and (*C*) 31 January using the PJ radar. Color-coded lines indicate known Z_e–S relationships for dry and wet snowflakes from the literature (13–17). Gray boxes represent Z_e–S ensemble with the 25th/75th percentile, whiskers extend to the 5th/95th percentile, and the median. Star symbols show the total area of the seeding lines reaching the ground.

then decreased to 60 km^2 at 0301 UTC (Fig. 4*B*, star symbols). Spatial distribution of precipitation and the accumulation amounts are all attributed to cloud seeding as radars and gauges observed no natural precipitation (Fig. 2*C* and *SI Appendix*, Movie S2).

On 31 January, most of the snow accumulated in the ROD ~20 to 50 km east of Packer John (Fig. 3*C*) with a total accumulation of 339,540 m^3 (275 ac ft) assuming the best-match Z_e–S relationship over an area of 2,410 km^2 through a ~25-min period resulting from two seeding legs or 24 min of cloud seeding. The total accumulations range from 222,051 to 335,863 m^3 (187,004 to 480,420 m^3) when considering the 25th and 75th (5th/95th) percentiles from the Z_e–S relationship ensemble resulting into an average difference of 20% (43%) compared to the best-match estimate. Due to the high winds of about 30 m s^{-1} at flight level, the lines remained in the ROD for only about 25 min with some of the precipitation from the lines falling outside of the ROD. The largest amount of snow over the shortest time and over the largest area was produced on this day compared to 19 and 20 January.

The total accumulation for each radar scan time ranged between 10,000 and 80,000 m^3 (8.1 and 64.8 ac ft) following the published Z_e–S relationships (13–17) (colored lines in Fig. 4*C*). For the Z_e–S ensemble, the 5th and 95th percentiles of accumulations ranged between 10,000 and 108,000 m^3 (8.1 and 87.5 ac ft) for each radar scan. Using the best match Z_e–S relationship shows total accumulations for each scan between 15,000 and 75,000 m^3 (12.2 to 60.8 ac ft) throughout the precipitating time period. The seeding lines coverage steadily increased from 830 km^2 to over 1,000 km^2 between 2110 and 2117 UTC, then remained above this value until 2135 UTC, and decreased to 400 km^2 at 2146 UTC (Fig. 4*C*, star symbols) as the lines propagated out of the ROD.

Conclusion

Snow accumulations from cloud seeding were quantified using precipitation gauge and radar analyses as seeding lines passed through the ROD in three cases. As the seeding lines passed over the precipitation gauges, snow accumulations attributed to cloud seeding ranged from 0.05 to 0.28 mm with precipitation rates of 0.4 to 1.2 mm h^{-1} (Fig. 2). Ground-based radar data were used to analyze the spatial distribution and estimate the total amount of snowfall from these seeding lines. During weaker wind conditions, such as on 19 and 20 January, precipitation associated with cloud seeding reached the ground within 50 km range from the release of the seeding material (Fig. 3). As seeding lines moved across the terrain, seeding lines widened and snowfall intensity increased as shown on 19 January (Fig. 3*A*). However, on 20 January most of the precipitation reached the ground before approaching the highest terrain. During strong wind conditions on 31 January, precipitation accumulated farther downwind over the higher terrain.

Cloud seeding generated the most amount of snow on 31 January when the strongest wind was observed with total accumulations of 339,540 m^3 (considering the best-match relationship) over only 25 min resulting from two seeding lines or 24 min of seeding. During the days with low wind speed, snow accumulated mainly within the eastern part of the ROD. On 19 January, a total of 123,220 m^3 of liquid equivalent snowfall generated by two seeding lines or 20 min of cloud seeding accumulated over 2,327 km^2. As the seeding lines propagated over higher terrain, snowfall was orographically enhanced. On 20 January, snow fell out more rapidly compared to 19 January accumulating mostly over a smaller area. Total accumulations generated by eight seeding lines or 86 min of cloud seeding over 160 min reached 241,260 m^3, double the amount observed on 19 January. The uncertainty in the total accumulation is related to the choice of Z_e–S relationship. Based on a Z_e–S relationship ensemble the total accumulation for all three seeding events can vary between 20% and 47% using 25th/75th and 5th/95th percentiles from the Z_e–S relationship ensemble.

Questions remain how cloud seeding efficacy depend on the type of cloud seeding operations, the amount of AgI released, and the temporal and spatial evolution of a variety of atmospheric variables that control microphysical and dynamical processes in clouds and precipitation affect. As a next step, we will quantify ice and snow production in these seeded clouds and study the environmental conditions and cloud dynamic and microphysical processes for the three cases presented here. These results are a fundamental step forward toward being able to answer the overall question about glaciogenic cloud seeding efficacy. These findings set the stage for validating numerical models that simulate the microphysical impacts of cloud seeding (2, 18) and improving interpretation of precipitation observations during cloud seeding operations. After that, the AgI seeding effect over a target can be quantified with more confidence at different time scales using the ensemble approach (9).

Materials and Methods

All data presented here are publicly available through the SNOWIE data archive website maintained by the Earth Observing Laboratory at the National Center for Atmospheric Research and the SNOWIE radar data archive maintained by the Center for Severe Weather Research (CSWR). Data are archived in NetCDF or ASCII format, and each \ contains an accompanying text file providing necessary metadata. Description of calibration and uncertainties for DOW and precipitation gauges are also provided in *SI Appendix*.

ACKNOWLEDGMENTS. We thank the crews from the Doppler on Wheels (DOW) radars from the CSWR and students from the University of Colorado, University of Wyoming, and University of Illinois for their help operating and deploying instruments during the campaign. Funding for CSWR-DOWs was provided through National Science Foundation (NSF) AGS-1441831. Funding for seeding aircraft was provided by Idaho Power Company. The research was supported under NSF Grants AGS-1547101, AGS-1546963, and AGS-1546939.

1. B. Vonnegut, The nucleation of ice formation by silver iodide. *J. Appl. Phys.* **18**, 593–595 (1947).
2. R. M. Rauber *et al.*, Wintertime orographic cloud seeding. *Appl. Meteor. Climatol* **58**, 2117–2140 (2019).
3. A. W. Huggins, Another wintertime cloud seeding case study with strong evidence of seeding effects. *J. Weather Modif.* **39**, 9–36 (2007).
4. A. B. Super, B. A. Boe, Microphysical effects of wintertime cloud seeding with silver iodide over the Rocky Mountains. Part III: Observations over the Grand Mesa, Colorado. *J. Appl. Meteorol.* **27**, 1166–1182 (1988).
5. A. B. Super, E. W. Holroyd, III, Some physical evidence of AgI and liquid propane seeding effects on Utah's Wasatch Plateau. *J. Weather Modif.* **29**, 8–32 (1997).
6. A. B. Super, J. A. Heimbach, Microphysical effects of wintertime cloud seeding with silver iodide over the Rocky Mountains. Part II: Observations over the Bridger Range, Montana. *J. Appl. Meteorol.* **27**, 1152–1165 (1988).
7. P. V. Hobbs *et al.*, Radar detection of cloud-seeding effects. *Science* **213**, 1250–1252 (1981).
8. M. J. Manton *et al.*, Further analysis of a snowfall enhancement project in the Snowy Mountains of Australia. *Atmos. Res.* **193**, 192–203 (2017).
9. R. M. Rasmussen, Evaluation of the Wyoming Weather Modification Pilot Project (WWMPP) using two approaches: Traditional statistics and ensemble modeling. *J. Appl. Meteorol. Climatol.* **57**, 2639–2660 (2018).
10. J. R. French *et al.*, Precipitation formation from orographic cloud seeding. *Proc. Natl. Acad. Sci. U.S.A.* **115**, 1168–1173 (2018).
11. S. A. Tessendorf *et al.*, A transformational approach to winter orographic weather modification research: The SNOWIE Project. *Bull. Am. Meteorol. Soc.* **100**, 71–92 (2019).
12. R. M. Rasmussen *et al.*, How well are we measuring snow: The NOAA/FAA/NCAR winter precipitation test bed. *Bull. Am. Meteorol. Soc.* **93**, 811–829 (2012).
13. K. L. Gunn, J. S. Marshall, The distribution with size of aggregate snowflakes. *J. Meteorol.* **15**, 452–461 (1958).
14. J. Imai, "Raindrop size distributions and the Z-R relationship" in *Proceedings of the Eighth Weather Radar Conference* (American Meteorological Society, Boston, MA, 1960), pp. 321–326.
15. R. S. Sekhon, R. C. Srivastava, Snow size spectra and radar reflectivity. *J. Atmos. Sci.* **27**, 299–307 (1970).
16. T. Puhakka, "On the dependence of the Z-R relation on the temperature in snowfall" in *Preprints, 16th Conference on Radar Meteorology* (American Meteorological Society, Boston, MA, 1975), pp. 504–507.
17. J. P. Wolfe, J. R. Snider, A relationship between reflectivity and snow rate for a high-altitude S-band radar. *J. Appl. Meteorol. Climatol.* **51**, 1111–1128 (2012).
18. L. Xue, Implementation of a silver iodide cloud seeding parameterization in WRF: Part 1: Model description and idealized 2D sensitivity tests. *J. Appl. Meteorol. Climatol.* **52**, 1433–1457 (2013).